ARTICLE

BIOTECHNOLOGY and BIOENGINEERING

# Design and Demonstration of a Pumpless 14 Compartment Microphysiological System

**Paula G. Miller, Michael L. Shuler**

Department of Biomedical Engineering, Cornell University, 113 Weill Hall, Ithaca 14853 New York; telephone: +1-607-280-2507; fax: +1-607-255-7330; e-mail: mls50@cornell.edu

**ABSTRACT:** We describe a human "Body-on-a-chip" device (or microphysiological system) that could be used to emulate drug distribution, metabolism, and action in the body. It is based upon a physiologically based pharmacokinetic–pharmacodynamic (PBPK–PD) model, where multiple chambers representing different organs are connected with fluidic channels to mimic multi-organ interactions within the body. Here we describe a pumpless 14 chamber (13 organs) microfluidic cell culture device that provides a separation between barrier and nonbarrier types of cell cultures. Our barrier chamber layer (skin, GI tract, and lung) allows for direct access and/or exposures to chemical or biological reagents forcing these reagents to pass through a barrier of cells established on a microfabricated membrane before exposing the nonbarrier tissue chambers (fat, kidney, heart, adrenal glands, liver, spleen, pancreas, bone marrow, brain, muscle) or entering the microfluidic circulation within the device. Our nonbarrier tissue chambers were created as three-dimensional configurations by resuspending cells in hydrogel (PGMatrix). We used cell lines to represent five of these organs (barrier lines—A549 [lung] and Caco2 [GI]) (nonbarrier lines—HepG2 C3A [liver], Meg01 [bone marrow], and HK2 [kidney]). The dimensions of our straight duct-like channels to each organ chamber were designed to provide the appropriate flow of a culture medium. The organ volumes and organ flow rates that have been reported for an average human male were used to estimate the desired fluid retention times in each organ chamber. The flow through the channels was induced by gravity on a custom programmed rocker platform which enabled pumpless operation and minimized bubble entrapment. The purpose of this paper is to describe the design and operation of a 14 chamber multi-organ system representing 13 tissues/organs with both barrier and nonbarrier tissue chambers and to study the interactive responses among the various cell lines. We demonstrate that five different cell lines survived with high viability (above 85%) for 7 days. We compared the individual observed flow rates to the compartments to the desired or estimated flow rates. This work demonstrates the feasibility of constructing, operating and maintaining a simple, gravity-driven, multi-organ microphysiological system with the capability of measuring cellular functions such as CYP1A1 and CYP3A4 activities, albumin release, urea, maintenance of tight junctions, and presence of surfactant for a sustained period.

Biotechnol. Bioeng. 2016;113: 2213–2227.



**KEYWORDS:** microphysiological systems; PBPK model; microfabrication; human surrogates; tissue engineered models; drug evaluation

## Introduction

Microphysiological systems or "Body-on-a-chip" devices have been proposed as in vitro systems to improve drug discovery and reduce dependency on animal studies in preclinical testing (e.g., Esch et al., 2014a; Sin et al., 2004; Sung et al., 2013). Preclinical testing of drugs using animals, particularly rodents, does not always predict the human response to drugs or chemicals. Only 11% of drugs that have passed through animal trials have been approved for human use (Cook et al., 2014). A human surrogate model that can be used to test potential drugs in preclinical studies would allow pharmaceutical firms to improve the determination of which drugs should move forward.

In vitro monolayer cultures have been used in initial screening of various chemicals to estimate responses to these chemicals, but the monolayers fall short of the complex body systems because they do not recreate the interactions that normally exist in an organism. Therefore, more physiologically realistic systems are required (e.g., Huh et al., 2012; Lin and Lu, 1997; Wagner et al., 2013). Various computer/mathematical models have been designed to improve the study of physiologically based pharmacokinetic–pharmacodynamics (PBPK–PD) based drug toxicity, mimic some multi-organ interactions and simulate parts of human metabolism (Gerlowski and Jain, 1983). Such mathematical models, by themselves, are limited because they cannot capture the full complexity of the biological system, but by combining them with experimental systems, such as "body-on-a-chip" systems, their usefulness can increase (Esch et al., 2014b; Shuler, 2012; Sung et al., 2013).

The 3D cell culture models typically are often better models of organ metabolism compared to monolayer culture systems, because the 3D models may better mimic cell differentiation, tissue

Correspondence to: M.L. Shuler
Contract grant sponsor: National Center for Advancing Translational Sciences
Contract grant number: UH2TR000156-01
Contract grant sponsor: National Science Foundation
Contract grant number: ECS-0335765
Contract grant sponsor: NIH
Contract grant number: 1S10RR025502
Received 27 July 2015; Revision received 25 March 2016; Accepted 4 April 2016
Accepted manuscript online 12 April 2016;
Article first published online 29 April 2016 in Wiley Online Library (http://onlinelibrary.wiley.com/doi/10.1002/bit.25989/abstract).
DOI 10.1002/bit.25989

organization, structural configuration, biochemical function, and dynamic mechanical properties of the system (Abbott, 2003; El-Ali et al., 2006; Greek and Menache, 2013; Huh et al., 2012; Lancaster et al., 2013; Sato and Clevers, 2013; Whitesides, 2006). By using hydrogels, scaffolds, or other platforms one can construct these 3D configurations to better mimic an organ's physiology resulting in more realistic models. However, functional assessment of organ response may require 2D cultures on cantilevers to measure force and use of micro-electrode arrays (MEA) to measure electrical activity (Natarajan et al., 2011; Smith et al., 2013). The fluid-to-cell ratios within the microfluidic devices are closer to physiological with 3D systems than in monolayer cultures and thus potentially better mimics of whole body response (Sung et al., 2013; Wagner et al., 2013).

Individual groups have designed 3D systems that focus on a single organ in a microfluidic device, such as liver, lung, heart, kidney, GI tract, and others (e.g., Bhatia and Ignber, 2014; Esch et al., 2015; Nakao et al., 2011; Nalayanda et al., 2009; Sung et al., 2013). These devices are able to incorporate multiple cell types from the desired organ at cell concentrations that are similar to what has been observed in vivo (Wagner et al., 2013). Others have started to create combinations of organs in their systems to observe organ to organ interactions (e.g., Esch et al., 2014a; Imura et al., 2010; Maschmeyer et al., 2015; Sin et al., 2004; Sung et al., 2013; Wagner et al., 2013; Zhang et al., 2009).

We believe that the design of in vitro mimics of the human body should be guided by the PBPK models (Ghanem and Shuler, 2000; Sung et al., 2014; Sweeney et al., 1995). A microscale cell culture analog ($\mu$CCA) is a type of microfluidic device that is based on a PBPK–PD model where multiple cell culture chambers are connected with fluidic channels to mimic multi-organ interactions and test drug toxicity in a pharmacokinetic-based manner. Examples of these body on a chip systems coupled to PBPK have been developed (e.g., Mahler et al., 2009; Sung and Shuler, 2009; Sung et al., 2010, 2014). Such devices have been used to test the efficacy or toxicity of naphthalene, doxorubicin, nanoparticles, and tegafur (Esch et al., 2014b; Sung and Shuler, 2009; Tatosian and Shuler, 2009; Viravaidya et al., 2004).

While most of the early systems required an external pump, we have developed "pumpless" systems because they are economical, can simplify set up and operation, operate with physiologically realistic shear stress (less than 2 dynes $cm^{-2}$) on cells, prevent bubble formation or entrapment and are versatile (Sung et al., 2010). In this paper, we describe a "pumpless" platform system that allowed for at least 14 chambers representing 13 different cell/tissue types or organs (note: two chambers are used for skin). Our pumpless 14 chamber device was designed by considering a number of factors: the PBPK model, overall physical device size, improving our choice of materials for the device, scaling the tissue/organ chambers so the proportions were more physiological than prior designs, having separate chamber layers for barrier and nonbarrier tissues, establishing some direct chamber to chamber communication through membranes, incorporating access ports to mimic external exposures to drugs or chemicals through barrier tissues (GI, lung, and skin), sterility, and ease of handling.

The fluid dynamics in multi-chamber devices are complicated and the manipulation of fluids in microsystems has been extensively reviewed for analytical systems (Morier et al., 2004). Slight changes in pressure difference between the inlet and outlet of a microsystem can have large effects particularly with a large number of flow paths (Perry and Chilton, 1973). The positioning of the device on the microfluidic-based analytical platform is also critical for accuracy (Morier et al., 2004). Morier presented a means of using gravity flow to induce linear convection within a microfluidic system. However, multichannel devices are difficult to analyze because there are many channels flowing at the same time into a common reservoir. Also, our channeled system was dependent on the layering of different types of materials to provide sealing (silicone gaskets), rigidity of channel walls (provided by using polymethylmethacrylate sheets [PMMA]), cell adherence and porosity (polycarbonate membranes). To obtain the flow rates of the various channels in our multi-channel devices we decided that another approach was necessary. For the initial design of the device described later, we used the Hagen–Poiseuille's equation to estimate the channel dimension to achieve the desired flow rate (Kirby, 2013). Then we analyzed our device's flow rates by observing the linear flow rate for each individual channel and compared the two values.

Our pumpless system used a gravity induced flow that was generated by using a programmable rocker platform to circulate fluid bidirectionally. We simplified our fluid dynamics by using straight channels across our chambers and calculated the channel sizes necessary to achieve desired flow rates. We used physiological values of fluid retention times for each organ of an adult human male as a guide. We determined that the calculated flow rates of channels were comparable to what we could observe through a video capturing technique. We then tested the 14 chamber device for its ability to sustain viability with a liver cell line (HepG2 C3A) in all of the chambers for 48 h and we were able to sustain cellular activity (viability and functionality) with five different cell lines in five different compartments for 7 days. All together these studies demonstrated the feasibility of this approach using a novel 14 chamber device with a liver cell line (HepG2 C3A) in all chambers and with five different cell lines in five of the chambers.

## Materials and Methods

### Cell Cultures and Media Used

The following immortalized human cell lines obtained from the American Type Culture Collection ((ATCC) (Manassas, VA)) were tested in the two layered pumpless device: (i) A human colorectal adenocarcinoma cell line (Caco2) maintained in Eagle's Minimum Essential Medium (EMEM) (ATCC cat# 30-2003) plus 20% fetal bovine serum (Invitrogen, Grand Island, NY, cat# 26140); (ii) a human lung carcinoma (A549) maintained in F-12 K medium (ATCC cat#30-2004) plus 10% fetal bovine serum; (iii) A human hepatocellular carcinoma cell line (HepG2 C3A) maintained in Eagle's Minimum Essential Medium plus 10% fetal bovine serum; (iv) A human kidney-papillomavirus 16 transformed cell line (HK2) maintained in Keratinocyte Serum Free Media plus 0.05 mg $mL^{-1}$ bovine pituitary extract and 5 ng $mL^{-1}$ human recombinant epidermal growth factor (Invitrogen #17005-042); and (v) A human bone marrow chronic myelogeneous leukemia cell line (Meg01) maintained in RPMI (ATCC #30-2001) plus 10% fetal bovine serum.

Cells were split or medium was refreshed every 3–4 days during normal maintenance. Confluent cell cultures were washed with Dulbecco's Phosphate Buffered Saline (DPBS), detached using 0.25% trypsin-0.53 mM EDTA solution (Invitrogen cat# 25200) or 0.05% trypsin-EDTA solution (HK2 cells only) and subcultured in culture flasks in a humidified incubator, at 5% $CO_2$ and 37°C.

The common circulating medium used for testing the pumpless device was EMEM plus 10% fetal bovine serum and was denoted as "Device Medium" and all of our experiments were done in this medium.

## Overall Device Description

The completely assembled μCCA device (Fig. 1[A1, B–D]) consisted of polycarbonate frame, two layers of 0.5 mm thick clear silicone gaskets (Sigma, St. Louis, MO, #GBL664571) for the cell/organ chambers, two layers of 0.25 mm thick polymethylmethacrylate (PMMA) gaskets (GoodFellow, Coraopolis, PA, #ME303005) for channels, porous polycarbonate nucleopore track-etch membranes with 0.4 μm pore size (Whatman, Clifton, NJ, cat# 111707), 1.6 mm thick silicone gaskets (Sigma #GBL664273), and eight stainless steel pan head phillips machine screws (thread size 4–40, length 3/4″) (McMaster-Carr, Aurora, OH, #91735A113) that held the platform together. The frame of this device was milled out of a polycarbonate sheet on a CNC Bridgeport Milling Machine. All materials (except PMMA) were autoclaveable, fairly inert, transparent, easy to manipulate, helped prevent leaking, and when assembled were not detrimental to cells. PMMA was not autoclaveable so its chemical sterilization was done separately from the rest of the system before assembly (see Device Preparation and Assembly Section). Figure 2A and B show photographs taken of the actual device with trypan blue rocked throughout the system.

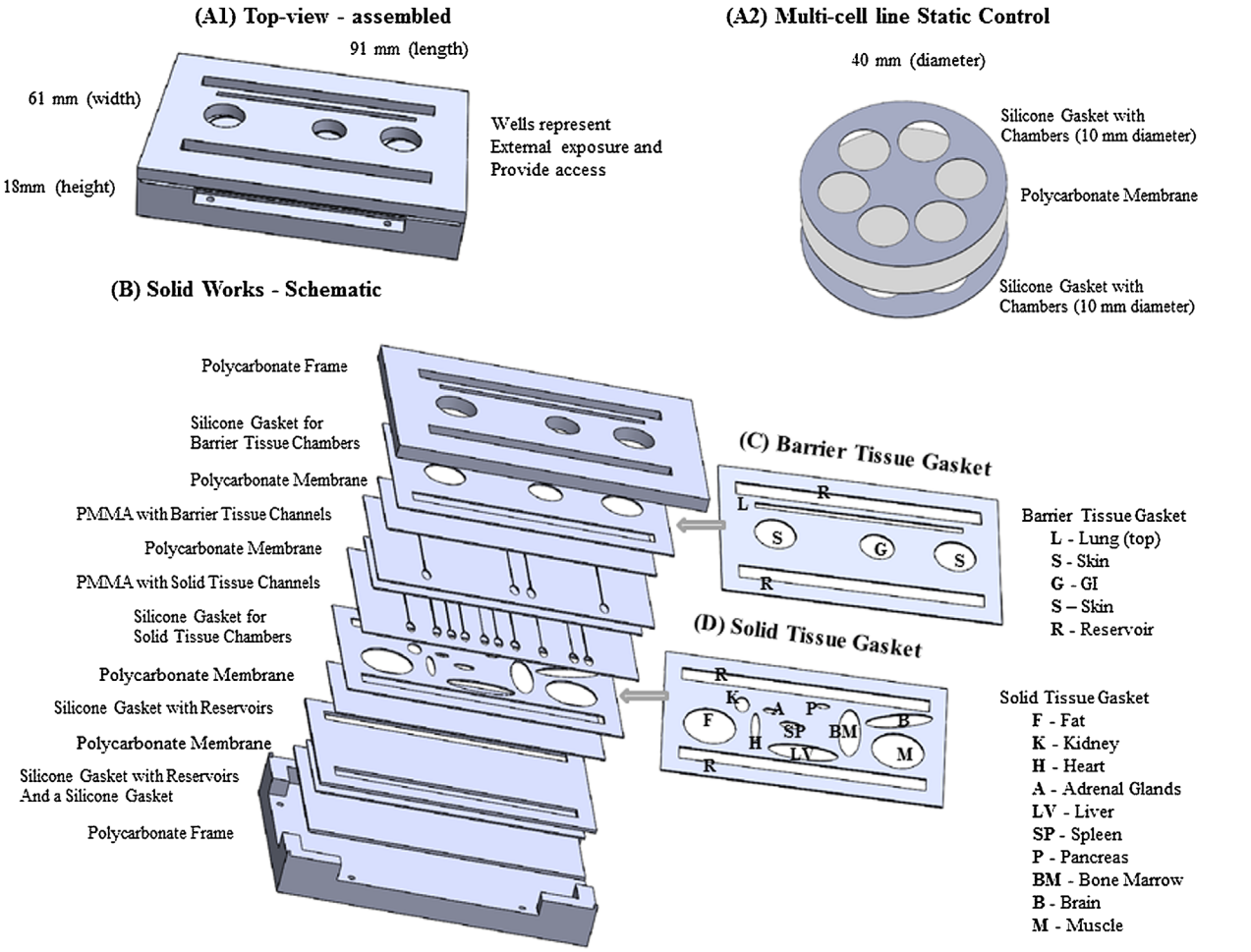


**Figure 1.** Schematic of a two layered pumpless Body-on-a-chip device. A 14 chamber device that has an external barrier tissue layer separate from a solid tissue layer. The 14 chamber chip consists of a series of clear silicone gaskets, polycarbonate membranes, PMMA layers and a polycarbonate frame that sandwiches the unit together. (**A1**) A Solid Work's diagram of the 14 chamber chip. The chip is held together with small stainless steel screws. The chambers of the chip are connected by individual channels to common reservoirs for culture medium distribution. The channels vary in size (Table II) and have been scaled down to represent the physiologic ratios of the average adult male's blood flow rates. There are open wells to provide direct access to specific chambers (barrier tissues—lung, skin, and GI tract) and reservoirs. (**A2**) A Solid Work's diagram of the chamber gasket used in the Multi-cell line Static Function Control. These gaskets were inserted into a 60 mm dish where the cells were plated as in the rocked device and maintained in the Device Medium with the same volume as the rocked device. (**B**) Solid Work's diagram of the assembled device (top-view). (**C**) Enlarged view of the barrier chamber gasket. (**D**) Enlarged view of the nonbarrier chamber gasket.

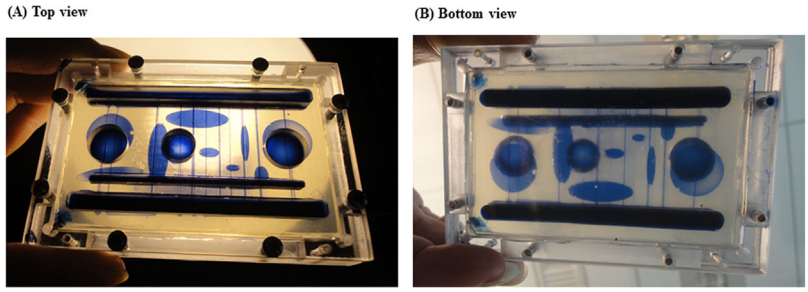


**Figure 2.** Actual Photographs of the two layered pumpless Body-on-a-chip (14 chamber device) (Barrier Tissue Layer and Solid Tissue Layer) with Trypan Blue flowing through the channels and chambers. The device was placed on a programmable rocker platform to create gravity-driven bidirectional flow. (**A**) Top-view. (**B**) Bottom-view.

## Device's Chamber Sizes and Chamber Descriptions

The average physiological human male organ volumes and flow rates to those organs have been previously determined from several sources (e.g., Brown et al., 1997; Davies and Morris, 1993; Haber et al., 2013; Price et al., 2003). The organ volumes for our device were scaled down proportionately from the average human male organ volumes reported by Price and Haber by a factor of 40,000 (Haber et al., 2013; Price et al., 2003). The smallest organ volume was set to a volume that was comfortable to pipet the cell/hydrogel mixture and the other organs were scaled to that value (Table I). This volume was 2.5 μL and corresponded to the size of the pancreas and adrenal glands. The volume of an organ (cell/hydrogel mixture) was used as a basis to calculate the volume of its chamber. The calculated chamber sizes were 20% larger than our organ volumes to provide adequate volume for fluid flow over the organ. The thickness of the chamber gaskets was 0.5 mm so the height of the organ was set to 0.4 mm. The width and length of the elliptic cylinder shaped chambers were calculated to fit within a length of 30 mm (space between the two reservoirs). The elliptical shape was chosen instead of a rectangular shape to help reduce dead flow spaces that could be created by corners. In this device, the chambers (muscle = 100 μL, fat = 90 μL) representing muscle and fat were scaled down by a factor of 320,000 rather than 40,000 because their relative sizes to the other tissues complicated the design of the prototypic device. The chambers designated for those two tissues were represented by using 1/8th of our estimated volumes (muscle total volume = 800 μL, fat total volume = 717 μL). However, the remaining 7/8th of these volumes could be incorporated into the bottom of the reservoirs (fat in one reservoir bottom and muscle in the other) to keep the device relevant physiologically.

The chambers and media reservoirs were made by using Corel Draw (Corel Corporation, Ottawa, ON) and the silicone chamber gaskets were cut with a VersaLaser VLS3.60 Cutting and Engraving $CO_2$ Laser (Universal Laser Systems, Scottsdale, AZ). The bottoms of the chambers or reservoirs were created by attaching a polycarbonate porous nucleopore track-etch membrane (0.4 μm pore size) to the silicone layer.

## Nonbarrier Chambers

Nonbarrier tissues were 3D constructs and in this design were based on cells embedded in a PGMatrix hydrogel which is a synthetic peptide-based material with 19 amino acid residues designed from spider silk and the trans-membrane segment of human muscle L-type calcium channel (PGmatrix DMEM Research Kit, Pepgel LLC, Manhattan, KS). Our 3D tissue hydrogel constructs were placed directly on a polycarbonate membrane that was sandwiched between a silicone chamber gasket and another gasket creating chambers for those cells. The 400 μm depth should insure adequate oxygen delivery throughout the gel for the cell density used in these systems. This density was somewhat less than that seen in real tissue. Our chamber design left a height of 100 μm (20%) above the non-barrier components for a culture medium to circulate. Also, please note that the heart chamber was designed to study responses of the cells and the action of the heart was not mimicked in this device.

Specifically, the chambers for the nonbarrier tissues were created by embedding the cells in the PGMatrix on the nonbarrier chamber gasket 4 days before the actual assembly of the device so the cells would be well acclimated to the matrix. The cell concentration for plating the non-barrier tissues was $10^7$ cells $mL^{-1}$ in PGmatrix so that only the pipetting volume changed accordingly. The cells were resuspended in this hydrogel by following the PGMatrix "Quick Start" User Guide (1:9 ratio of the two components: PGworks solution to PGmatrix-DMEM solution for resuspending the cells), plated in their chamber quickly, incubated for 30 min at 37°C, 200 μL medium was added, then incubated for another 30 min and repeated twice before filling the dish with medium. This process produced a 0.5% (w/v) PGMatrix hydrogel; drying out was avoided by adding medium and the cells were allowed to adhere in the gel.

## Barrier Chambers

The chambers for external barrier tissues (GI tract, lung, and skin) were located above the nonbarrier tissues and the frame of the device was cut producing open wells so that there was direct access to these barrier chambers. The lung chamber was designed to span the width of the device so all chambers could be affected by this chamber; this design allowed us to direct all of the medium to the lung for aeration and then circulated to the rest of the device. This design also enabled external exposures to the lung cells first before entering the system. We designed two barrier chambers (25 mm in diameter) for the skin because

**Table I.** Physiological information, calculations used to compare and characterize the 14 chamber device.

| Organs | Organ volumes from literature (liters) | Device organ volumes (μL) | Flow rate from the literature (liters/min) | Residence time (min) | Channel X-sectional area ($mm^2$) | Calculated flow rate desired (μL/s) | Calculated linear flow rate desired (mm/s) |
|---|---|---|---|---|---|---|---|
| Lung | 1.01 | 25.3 | 2.44 | 0.41 | 0.173 | 1.02 | 5.90 |
| Skin[a] | 3.71 | 48.5 | 0.45 | 8.24 | 0.054 | 0.10 | 1.85 |
| GI tract | 1.23 | 30.8 | 0.93 | 1.32 | 0.107 | 0.39 | 3.64 |
| Fat[b] | 28.7 | 89.7 (627.6 μL in reservoir) | 0.57 | 50.3 | 0.011 | 0.03 | 0.36 |
| Kidneys | 0.32 | 8 | 1.17 | 0.27 | 0.120 | 0.49 | 4.08 |
| Heart | 0.36 | 9 | 0.73 | 0.49 | 0.095 | 0.30 | 3.16 |
| Adrenal glands | 0.1 | 2.5 | 0.011 | 9.09 | 0.012 | 0.01 | 0.83 |
| Liver | 1.57 | 39.3 | 1.32 | 1.19 | 0.127 | 0.55 | 4.33 |
| Spleen | 0.22 | 5.5 | 0.22 | 1.00 | 0.052 | 0.09 | 1.73 |
| Pancreas | 0.1 | 2.5 | 0.06 | 1.67 | 0.027 | 0.03 | 1.11 |
| Bone marrow | 1.59 | 39.8 | 0.48 | 3.31 | 0.077 | 0.20 | 2.60 |
| Brain | 1.34 | 33.5 | 0.68 | 1.97 | 0.091 | 0.28 | 3.08 |
| Muscle[c] | 32 | 100 (700 μL in reservoir) | 0.95 | 33.7 | 0.014 | 0.05 | 0.46 |

Physiological human male organ volumes from the literature (Haber et al., 2013; Price et al., 2003) compared to our device organ volumes. The flow rates from the literature (Haber et al., 2013; Price et al., 2003) and the male organ volumes were used to calculate the residence times. Residence time = organ volume/flow rate. The channel dimensions were estimated by using the Hagen–Poiseuille's equation, then the channel's crosssectional areas, volumetric flow rates (desired) and linear flow rates (desired) were calculated for the device held at a 5 degree angle. The numbers in the parenthesis represent the total volumes needed to make up for the amount lacking in the larger organ chambers (fat and muscle) and could be addressed by plating that volume in the bottom of the reservoirs. Please note that there are two chambers for the skin, therefore, the total volume is represented.

[a]There are two chambers set up for Skin. The volume pipetted into each of these chambers was 48.5 μL so the total volume for skin would equal 97 μL.

[b]The Fat chamber in the device contained 1/8th of the desired device volume that was calculated from the literature. So the values in parenthesis represent the volume that was placed in the bottom of a reservoir to make up the difference.

[c]The Muscle chamber contained 1//8th of the desired device volume that was calculated from the literature so the values in parenthesis represent the volume that was placed in the bottom of a reservoir to make up the difference.

preparing the cells in transwells (25 mm diameter) before assembly would be easier to insert into the device than handling a larger membrane.

The external barrier tissue chambers were created by resuspending the cells at a concentration of $3 \times 10^5$ cells $mL^{-1}$ in Device Medium using the calculated volumes and plating them on a membrane that was adhered to a silicone gasket for barrier tissues. These cells were allowed to incubate for 30 min at 37°C, then a small amount of medium was added gently to prevent drying, incubated again for another 30 min, and then after attachment, more medium was added to the dish. These membranes were cultured for 20 days to form a barrier layer before assembly. The design for the barrier chambers provided an apical and a basolateral side for each chamber and was designed to allow the passage of medium or a chemical(s) across that barrier.

## Device's Fluid Volumes and Channel Calculations

The channels to feed the chambers were made out of polymethylmethacrylate sheets (PMMA—0.25 mm thick) that was also designed in Corel Draw and cut with the laser. The channel sizes were determined by the following method. The residence time of each organ was calculated using the organ volumes and flow rates from Price and Haber (Table I) (Haber et al., 2013; Price et al., 2003). The residence time was the key parameter in determining the extent of reaction in each chamber. The hydraulic radius, surface area of each channel, desired volumetric flow rate, and desired linear flow rate were calculated (Table I). Since the channel shape was rectangular and the depth was fixed as 0.25 mm (thickness of the PMMA) the desired channel width could be determined.

The individual channel fluid volumes, chamber fluid and matrix volumes, and reservoir fluid, and matrix volumes were calculated to estimate a Fluid to Matrix ratio of 2.6 (Table II). The total fluid volume in the device was 4700 μL and the total matrix volume in the device was 1810 μL. These values are higher than the physiologic ratio of circulating fluid to cell mass in the average human by about fivefold. We were able to scale down cell masses and their flow rates proportionally by using the reported values for an average human male (Haber et al., 2013; Price et al., 2003).

The following formulas were used to calculate the approximate channel width needed to provide the flow rates that were close to the scaled physiological rates:

Residence Time = Organ volume/Flow rate

$$\tau = V/Q \tag{1}$$

where $\tau$ is the residence time (s), $V$ is the organ volume ($m^3$), and $Q$ is the flow rate ($m^3\,s^{-1}$).

$$Q = (\rho g \pi/8\eta)^* \left(\Delta h (R_H)^4/(L)\right) \tag{2}$$

where $Q$ = volumetric flow rate ($m^3\,s^{-1}$); $\rho$ = density of the media (1,009 g $m^{-3}$); $g$ = gravitational constant (9.8m $s^{-2}$); $\Delta h$ = height difference ($L^*\sin[5°]$), (m); $R_H$ = hydraulic radius of the channel

**Table II.** Estimated fluid volumes, hydrogel volumes, and channel flow rates in the 14 chamber device.

| Organs | Calculated channel fluid volume (μL) | Calculated chamber fluid volume (μL) | Pipetted PGMatrix volume (μL) | Calculated linear flow rate (mm/s) | Observed linear flow rate (mm/s) | Calculated flow rate (μL/s) | Observed flow rate (μL/s) |
|---|---|---|---|---|---|---|---|
| Lung | | 5.1 | 25.3 | 5.90 | | 1.02 | |
| Skin | 3.0 | 19.4 | 97 | 1.85 | 1.81 ± 0.56 (ave of 2) | 0.10 | 0.10 (ave of 2) |
| GI tract | 2.99 | 6.2 | 30.8 | 3.64 | 3.57 ± 0.90 | 0.39 | 0.38 |
| Fat | 2.34 | 17.9 | 89.7 | 0.36 | | 0.03 | |
| Kidney | 3.36 | 1.6 | 8 | 4.08 | 4.46 ± 1.69 | 0.49 | 0.54 |
| Heart | 2.65 | 1.8 | 9 | 3.16 | 5.95 ± 0.87 | 0.30 | 0.57[a] |
| Adrenal glands | 0.33 | 0.5 | 2.5 | 0.83 | 1.21 ± 0.44 | 0.01 | 0.01 |
| Liver | 3.56 | 7.9 | 39.3 | 4.33 | 4.1 ± 0.90 | 0.55 | 0.52 |
| Spleen | 1.46 | 1.1 | 5.5 | 1.73 | 3.27 ± 0.17 | 0.09 | 0.17[a] |
| Pancreas | 0.76 | 0.5 | 2.5 | 1.11 | 2.11 ± 0.87 | 0.03 | 0.06[a] |
| Bone marrow | 2.15 | 8.0 | 39.8 | 2.60 | 3.51 ± 1.00 | 0.20 | 0.27[a] |
| Brain | 2.56 | 6.7 | 33.5 | 3.08 | 2.69 ± 0.40 | 0.28 | 0.24 |
| Muscle | 3.02 | 20 | 100 | 0.46 | | 0.05 | |
| Reservoirs | | 4,610 | 627.6 + 700 = 1,327.6 | | | | |
| Total volumes | | Fluid volume (μL) | Matrix volume (μL) | | | | |
| | | 4,734.9 | 1,810.5 | | | | |

The total fluid volume of all the channels together was calculated as 28.18 μL, the total fluid volume in the chambers was calculated as 96.7 μL, the reservoirs can contain from 4,112 μL (minimum) to 5,112 μL (maximum) of fluid (our experiments used 4,600 μL in the reservoirs). The grand total of fluid in the device was calculated to be 4,237 μL (minimum) to 5,237 μL (maximum) (our experiments used 4,700 μL). The total chamber hydrogel volume was 482.9 μL and the total reservoir hydrogel volume was 1,328 μL. The grand total of hydrogel in the device was calculated to be 1,811 μL. The fluid to matrix ratio was calculated to be 2.3 (minimum) or 2.9 (maximum) (our ratio = 2.6). The individual channel volumetric and linear flow rates were calculated and we compared the calculated to the observed linear flow rates.

[a]The observed flow rates to these chambers are higher than the desired flow rates (calculated).

(m); $\eta$ = fluid viscosity (0.001011Pa*s); $L$ = Length of the channel (m).

Equation (2) was then solved for the hydraulic radius to give the desired flow. This value of $R_H$ was then used to calculate the corresponding channel surface area, SA.

$$SA = \pi(R_H)^2 \quad (3)$$

Since the channel's SA is actually rectangular this value of SA was used to estimate the appropriate values of one (height of the channel) and w (width).

Overall, the fluid flow of the μCCA device consisted of a two layer system made up of parallel channels with selected chambers having their channels separated by the polycarbonate porous membrane to allow controlled communication between compartments (e.g., first pass effects on the liver for orally delivered chemicals). Fluid motion in the overall device occurred by using a custom designed rocking program on an Infinity Rocker Platform (NextAdvance, Averill Park, NY, #IR103 with customized programs). Recirculation of the cell culture medium was achieved by a gravity-induced bidirectional flow (Fig. 2). Various rocking patterns were tested to determine which program would work the best. The programs used for these experiments were 30 or 60 s with one side in the highest position, flip, 30 or 60 s with the other side in the highest position, respectively, and repeat. The time to flip positions was very short (less than a second). This program provided predictable fluid flow and also ensured that the channels and reservoirs always contained fluid.

## Device Preparation and Assembly

Most of the device parts were autoclaved in 150 mm glass petri dishes (black spots were placed on one side of all gaskets to help with alignment and to make assembly easier). Kimwipes were placed in the bottom of the 150 mm dishes to prevent the gaskets from sticking to the bottom the dishes during autoclaving. Various layers were autoclaved together to streamline and make assembly easier. For example, a reservoir silicone gasket was layered with a polycarbonate membrane and a silicone chamber gasket to create the nonbarrier chambers. The autoclaving of these layers together helped to adhere the layers, helped maintain alignment, and decreased difficulty during assembly. Also, an extra silicone gasket was initially attached to the top of the top frame to prevent contamination during assembly. This gasket was removed after the device was assembled and secured with eight stainless steel screws. Then the device was placed in a sterile dish so the barrier chambers and reservoirs would be open. Extra 150 mm dishes were autoclaved because they were used as working platforms for assembly and the device was also placed into one 150 mm dish for incubation and maintaining sterility. Autoclaved forceps were used for handling and manipulating the layers; therefore, the cultures that were plated in the chambers could be picked up intact.

PMMA was chosen for the channel gasket rather than silicone because it was more rigid and maintained the channel shape better than the silicone channel gasket. However, PMMA could not be autoclaved. PMMA gaskets were soaked in 10% Clorox for at least 30 min and then rinsed 3× in DPBS (Invitrogen #14190) with Penicillin-streptomycin (100 U $mL^{-1}$; 100 μg $mL^{-1}$) (Invitrogen #15140-122) before assembly of the device to prevent contamination and provide wetting of the channel gasket.

The device was assembled from the bottom-up and medium was added before adding each layer to help minimize bubbles. After the device was assembled, the gently pipetting of medium into the reservoirs released any remaining bubbles. The device was then placed into a sterile 150 mm dish incubated in a humidified

incubator, at 5.0% $CO_2$ and 37°C. The assembly of this device was difficult because sterility needed to be maintained. We were able to maintain this sterility by covering the top frame with a gasket during the manipulations, adding medium, and after screwing the device together removing the gasket from the top frame. Also, the device was incubated in a sterile secondary container (150 mm petri dish) to keep the open chambers safe from contamination. The barrier chambers and the reservoir were open/exposed to the incubator atmosphere while in the petri dish.

### Fluid Dynamics of the System

The flow distribution studies were done to check the overall flow rates versus predicted values. First, the nonbarrier chambers were set up with hydrogel without cells and incubated for 30 min at 37°C. Then, the device was assembled using Device Medium, bubbles were eliminated by pipetting gently across the channel entrances and one sample (50 μL) from each reservoir was taken for a zero reading. Then 1.0 mL was removed from one of the reservoirs and 1.0 mL of 0.4% trypan blue (Sigma cat# T8154) was added. The device was set in motion on the rocker (30 s ($n = 5$) or 60 s ($n = 3$) with one side up then 30 or 60 s with the other side up, respectively). These studies were accomplished using multiple devices setup over several days. Samples of 50 μL were taken from the both reservoirs at 30 s, 1 min intervals for the next 30, and 60 min. The samples were place into a 96 well plate and absorbance was read in a VERSAmax microplate reader (Molecular Devices, Sunnyvale, CA) at a wavelength of 650.

When the distribution study (30 s trial) was completed, a clearance study ($n = 5$) was done on the same device. To start, a zero reading (50 μL) was taken from each reservoir. Then 500 μL was removed from each of the reservoirs and replaced with 500 μL of fresh medium. The device was set in motion (30 s with one side up then 30 s with the other side up). 50 μL samples were taken from both reservoirs at 30 s, 1 min intervals for the next 30, and 60 min. After each 1 min sample was taken, another 500 μL was removed from each reservoir and replaced with 500 μL of medium up to 10 min. The samples were place into a 96 well plate and the absorbance was read in a VERSAmax microplate reader at a wavelength of 650.

The individual flow rate studies ($n = 5$) were done to measure the individual flow rates for certain channels. Flow in 11 channels was measured (skin, kidney, heart, adrenal glands, liver, spleen, GI tract, pancreas, bone marrow, brain, and another skin). Because the view of the other channels (lung, fat, and muscle) was obstructed, we were unable to measure flow individually in those channels.

The flow rate studies were initially set up the same way as the flow distribution studies. The hydrogel was incubated for 30 min in the chambers to represent the presence of the tissue. Then the device was assembled using medium, bubbles were cleared, video camera set up, and rocker platform placed with one side in the highest position (5 degree angle) for the reported measurements, although preliminary data were obtained for smaller angles (e.g., 1 degree). The device was placed on the rocker, video was started and then 1 mL of 0.4% trypan blue was added to the reservoir that was in the highest position. The device was not rocked during this study because each experiment was completed within 30 s (finished before one rock cycle would occur). We used Screenpresso (www.screenpresso.com) to capture the photographs from the video for the first 10–15 s, then ImageJ (rsb.info.nih.gov/ij/download.html) was used to measure the distance that the dye traveled down the channel and Microsoft Office Excel 2007 (www.microsoft.com) to calculate the average linear flow rates.

### Preliminary Cell Culture Studies

We grew five different cell lines in each other's medium to determine what medium to use for our rocked device. All five cell lines grew satisfactorily in the various mediums and displayed normal cell morphology so we chose EMEM plus 10% FBS as our "Device Medium." We chose this medium for further experiments since it was relatively inexpensive.

Then studies were done to compare hydrogel embedded cultures (grown in PGMatrix and "Device Medium") to cultures grown as monolayers in six well plates. The cultures were observed and viability testing was done to determine if PGMatrix (at our desired volumes) could be used without detrimental effects. Viability was assessed by using two methods (trypan blue [Sigma cat# T8154] exclusion and Invitrogen Live/Dead Stain [Invitrogen #L3224]) because we wanted to know if the Live/Dead Stain could be used instead of trypan blue exclusion. When using trypan blue one must obtain a single cell suspension and that would be difficult to do with the rocked device. Viability was determined as described in the Supplemental Materials (using modified manufacturer's procedures). This preliminary study ($n = 3$) demonstrated that the nonbarrier cells could survive in the PGMatrix (at our desired volumes) for at least 11 days hence survival in the device was anticipated. Trypan blue and Live/Dead Staining comparison demonstrated that these viability methods were comparable in our laboratory therefore using the Live/Dead Stain to determine viability in our device would be acceptable (data not shown).

## Cell Line Compatibility, Viability, and Function in the Rocked Device

### Viability Studies in the Device

A preliminary study was done to determine if we could grow cells adequately in all 14 chambers of our device. We plated one cell line in all of the chambers after being resuspended in PGMatrix ($n = 3$). Specifically, the HepG2 C3A cell line was resuspended in PGMatrix (see above—nonbarrier chambers), plated (varying volumes) in all 14 chambers of the rocker device's chamber gaskets, Device Medium was added to the dish after cell attachment, and the cells were allowed to grow for 4 days. The gaskets were assembled on day 4 into the device and allowed to rock for 48 h. After 48 h, viability was determined by using the Live/Dead Stain.

After the preliminary viability tests, five different cell lines were cultured simultaneously in the device to test for any differences in viability, cellular response, potential interactions, and overall compatibility when compared to simultaneous culture of all five cell lines in a static control.

The cell lines used for barrier tissues (Caco2 and A549) were maintained in the suggested medium, trypsinized, and the cell

concentration was adjusted to $3 \times 10^5$ cells $mL^{-1}$ in the Device Medium. The 2D tissue constructs were plated as described previously in their appropriate chamber that was created by adhering a polycarbonate membrane to the barrier chamber gasket. These cells were maintained in 150 mm dishes for 20 days before the actual assembly of the device so the cells would be well attached, confluent, and barrier properties obtained as determined by Mahler (Mahler et al., 2009). Medium was refreshed every other day by removing 50% of the spent medium and replacing it with fresh medium until the device was assembled. The whole barrier chamber gasket was transferred into the device with sterile forceps on the day of assembly or transferred into a 150 mm petri dish to be used as a control.

The cell lines used for nonbarrier tissues (HepG2 C3A, HK2, and Meg01) were maintained in their suggested medium, trypsinized, and the cell concentration adjusted to $10^7$ cells $mL^{-1}$ in PGMatrix. The 3D tissue constructs were plated as described previously in their appropriate chambers. These cells were maintained in 150 mm dishes for 4 days before the actual assembly of the device so the cells would be well adapted. Device Medium was refreshed every other day by removing 50% of the spent medium and replacing it with fresh medium until the device was assembled. The whole nonbarrier chamber gasket was transferred into the device with sterile forceps on the day of assembly or transferred into a 150 mm petri dish with the cells on the barrier chamber gasket as a control.

Devices were assembled using a barrier chamber layer (20 days) and a nonbarrier chamber layer (4 days) that were cultured separately, along with channel gaskets, sealing gaskets, and membranes. After the device was assembled, the flow of device medium was started (by rocking), and fed every day for 7 days by replacing 50% of the spent medium of the reservoirs and open wells with fresh medium. After 7 days viability was determined by using the Live/Dead Stain as described earlier ($n = 3$). Static Viability Controls were assembled from a barrier chamber layer and a nonbarrier chamber layer that were cultured separately. The layers were placed in a 150 mm petri dish together in Device Medium, and fed every day for 7 days by replacing 50% of the spent medium. The total volume of device medium (60 mL) in the Static Viability Control was much higher than the total volume of device medium (4.7 mL) in the device. The excess medium in the Static Viability Control was necessary to cover both gaskets at the same time and to insure that the viability in the Static Viability Control would be maximal. The static viability (using the Live/Dead Stain) was then compared with that of the rocked system.

## Function

The rocked devices (three per experiment) were assembled as described above (4.7 mL per device) but two types of controls were used to measure cellular function. The Static Viability Control that we used previously had a large volume (60 mL) that would dilute any released compounds. Therefore, urea, albumin, and P450 enzyme concentrations could be diluted and not be detected because the levels would be below the sensitivity of our assays. The two types of static controls that we used to study function were denoted as: (i) Single-cell line Static Function Controls. Basically, two 6 well plates were used per cell line where each cell line was plated as a monolayer or embedded in PGMatrix onto 25 mm circular glass coverslips (Fisher, Birmingham, AL, #12-546 25cir-2) and grown in six well plates (VWR, Radnor, PA, #15705-056) (2 mL Device Medium per well). (ii) Multi-cell line Static Function Control (three per experiment). Here, each cell line was plated as a monolayer or embedded in PGMatrix into their individual chamber as in the device. The chambers were created by sandwiching a porous polycarbonate nucleopore track-etch membranes (0.4 μm pore size) between two layers of 0.5 mm thick clear silicone gaskets with cell/organ chambers. The silicone gaskets were designed using Corel Draw and cut with the VersaLaser (Fig. 1A2). The diameter of these silicone gaskets was 40 mm so they would fit into a 60 mm petri dish (4.7 mL Device Medium per dish). Cells were prepared in the same way as for the device and, as in the device experiments, 50% of the medium was refreshed every other day before assembly and then every day for 7 days following assembly.

## Urea and Albumin Synthesis

Cell culture medium (1 mL) was collected and frozen at −80°C from each device and each static control once a day for 7 days with day 1 corresponding to 24 h after of the device's assembly. Urea concentrations in the medium were measured using a DIUR assay kit (BioAssay Systems, Hayward, CA, QuantiChrom catalog #DIUR-500). We transferred 50 μL of medium into the wells of a 96 well plate, added 200 μL chromogenic reagent that forms a stable colored complex specifically with urea, incubated for 20 min at room temperature and measured the optical density at 520 nm using a spectrophotometer. The results were compared to a standard curve and are expressed as mg/dL.

Albumin synthesis was evaluated by Enzyme-Linked Immunosorbent Assay (ELISA), using a kit and following the manufacturer's directions (Bethyl Laboratories, Inc., Montgomery, TX, catalog # E80-129), see Supplemental Materials for details. The results were compared to a standard curve and expressed as μg/mL.

## P450 Enzyme Activity

CYP450 enzyme activity was determined using Promega Glo assays (Promega Corp., Madison, WI, catalog #V9002 for CYP3A4 and catalog #V8752 for CYP1A1) following the manufacturer's instructions, see Supplemental Materials for details. The results were compared to a standard curve and expressed as nM. Results from the induced groups were compared to the uninduced control groups (not treated with induction reagents). For each induction experiment, one separate device was used for control, and two devices were induced in parallel for the enzymes, producing two technical replicates per enzyme.

## Immunostaining

At the end of the 7-day cell culture period, the devices were disassembled and the cells were fixed for 10 min in 4% paraformaldehyde at room temperature. Following a 30 min wash with PBS plus 5% FBS, we permeabilized the cells by applying 0.25% Triton X-100 in PBS for 10 min at room temperature and

blocked the cells with PBS containing 5% of bovine serum albumin (BSA) for 60 min at room temperature. The cells were labeled with ZO-1/TJP1 monoclonal antibody with FITC conjugate (ThermoFisher, Waltham, MA, #33-9111) diluted to 1 μg/mL in PBS containing 5% BSA. After 1 h of incubation, we washed with PBS plus 5% FBS two times for 5 min and permeabilized again with 0.1% Tween 20 (Sigma #P2287) in PBS for 20 min. After washing three times with PBS, the cells were blocked for 30 min in PBS containing 10% BSA and incubated with rabbit polyclonal anti-surfactant protein A (Millipore, Billerica, MA, #AB3420)(diluted 1:200 in PBS containing 10% BSA) for 60 min at room temperature. After the wash steps, the cells were incubated with goat anti-rabbit IgG–Rhodamine (Millipore #AP132R) (diluted 1:100 in PBS containing 10% BSA) for 60 min in the dark at room temperature. Finally, the cells were washed with PBS and mounted with Fluoroshield mounting medium with DAPI (Sigma #F6057) to stain the nuclei. Fluorescence was observed using the water immersion 25× objective on a Zeiss confocal microscope (Zeiss 710) and further magnified with the Zen program.

### Statistical Analysis

Data represent means of the experiments ± standard errors. Multiple means were compared with a two tailed Student *t*-test. Comparison of the means was ultimately made for the device against the Multi-cell line Static Function Control and was performed using Student's *t*-test. A *P*-value of $<0.05$ was considered to be significantly different.

## Results

### Flow Distribution

Flow Distribution experiments were performed on the 14 chamber chip adding trypan blue to one reservoir and measuring absorbance ($\lambda = 650$) in both reservoirs. The results (Fig. 3) indicate that the equilibrium between reservoirs using a high concentration of dye was not obtained by using the 30 s with one side up and then 30 s with the other side up rocking method. This result was determined after plotting the sample absorbance of five experiments. Figure 3A shows the observed overall dye distribution in the device over time for 30 min and then the final value at 60 min with standard error bars for each time point. The dye distribution experiments were then repeated using a 60 s with one side up and then 60 s with the other side up rocking protocol to see if equilibrium could be reached. The overall dye distribution results ($n = 3$) were plotted for the 60 s flip method, see Figure 3B. The results from the 60 s flip method gave a quicker overall response, reservoirs reached equilibrium and provided an improved dye distribution.

Clearance experiments were performed on the 14 chamber chip at the end of Flow Distribution Experiments. Samples were taken from both reservoirs at various time points to determine if trypan blue could be removed from the system. Figure 3C shows the time dependent absorbance ($\lambda = 650$) of trypan blue when 500 μL fresh media was added to each reservoir every minute. It was observed that trypan blue was cleared from our system (in all five trials). The results demonstrate that trypan blue can be removed from the system in less than 10 min. Please note that the end clearance of the device did not go to zero. The Device Medium was used to run the experiment and had a background absorbance of its own ($0.039 \pm 0.001$).

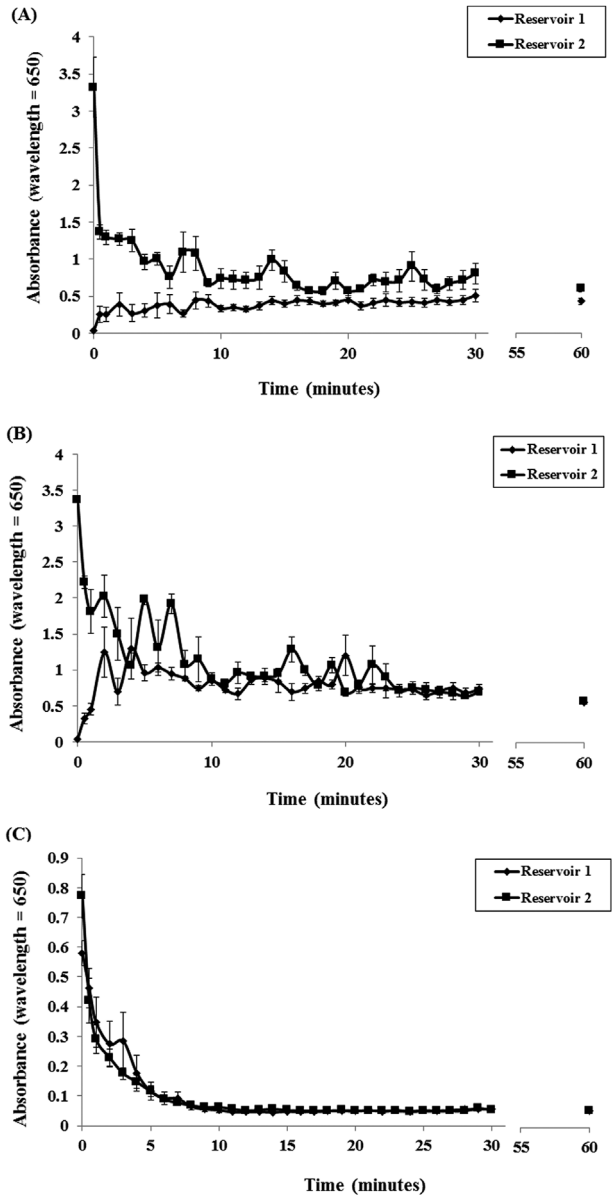


**Figure 3.** Overall Dye Distribution in the Rocked 14 Chamber Device. The overall dye distribution or clearance capability was determined after adding trypan blue to one reservoir and taking samples or removing reservoir medium from both reservoirs, adding Device Medium (500 μL every minute to each reservoir) and taking samples, respectively. The devices were set in motion on a programmable rocker platform and 50 μL samples were taken from each reservoir at 30 s, every minute for 30 min and then again at 60 min. Samples were measured for absorbance due to trypan blue at a wavelength of 650. (**A**) Overall dye distribution after adding trypan blue to one reservoir (30 s splits) ($n = 5$). (**B**) Overall dye distribution after adding trypan blue to one reservoir (1 min splits) ($n = 3$ (**C**) Clearance capability was determined (30 s splits) ($n = 5$). Data are means + SEM.

Individual channel flow rates were estimated by capturing photographs from videos of five independent flow experiments for at least 10 s. ImageJ was used to measure the distance that the dye traveled down the channel and the total length of a channel. The overall channel length which was the same for all of the channels and the measurements of the observed distances that the dye traveled were converted into millimeters. Multiple measurements for each channel were made over the course of each experiment. The average of these measurements minus the first second's measurement was recorded as the estimated average distance traveled per second (linear flow rate). The first second's measurement was removed to minimize any initial channel entrance effects. Table II compares the calculated linear and volumetric flow rates (desired) to the observed linear flow rates and calculated volumetric flow rates. Generally there was good correspondence between predicted and observed flow rates except for heart, spleen, pancreas, and bone marrow where the observed flow was higher than the calculated desired flow.

## Cell Viability

Preliminary viability experiments ($n = 3$) were done to make sure all of the chambers of the device could sustain viable cells (HepG2 C3A cells) for at least 48 h. The viability was determined by using Invitrogen's Live/Dead Stain. All 14 chambers had viability above 85% indicating that the supply of oxygen and the nutrients was acceptable for cell survival throughout the device. This experiment demonstrated that a 14 chamber system on the rocker platform could support high cell viability throughout the system (data not shown).

Experiments ($n = 3$) were done to test if five different cell types could survive in the system (Fig. 4) together for 7 days. The rocked device 7 day viability was compared to the viability of a Static Viability Control where the different cell lines were grown in the appropriate chambers of the device's chamber gaskets, placed next to each other in the same 150 mm petri dish and maintained together for 7 days. The cell lines that were chosen to complete this study were Caco2 to represent the GI tract, A549 to represent lung, HepG2 C3A to represent liver, HK2 to represent kidney, and Meg01 to represent bone marrow. Figure 5 compares the viability after 7 days of the Static Viability Control (five cells lines grown under static conditions in chambers of the two chamber gaskets in a 150 mm sterile petri dish) versus in the rocked device. Standard errors were calculated and there was no significant differences observed between Static Viability Control and rocked device viability for the individual cell lines. These results demonstrated that viability in the device with flow was equivalent to that observed in a static condition even though the static control's total volume of medium was almost 13-fold higher than that of the device. Micrographs of the cells that were maintained as static controls and in rocked device were taken to determine viability and for comparison using the fluorescent microscope, see Figure 5A and B.

## Functional Measurements

We measured albumin and urea synthesis throughout the 7-day exposure of the rocked device with bidirectional fluidic flow versus multi-cell line and single-cell line static function conditions, finding that there was an increase in albumin production that was significantly different when compared to static cultures (Fig. 6A). Average values of albumin production in the rocked device were significantly different from the Multi-cell line Static Function Control on days 4–7. Albumin production for the Multi-cell line Static Function Control started to decrease on day 6 and 7 which differed from the results with the rocked device. The average values of the Single-cell line Static Function Controls were, as expected, significantly lower than the rocked device or Multi-cell line Static Function Control. The HepG2 C3A Static Function Control was not significantly different from the Multi-cell line Static Function Control on days 1–5 but showed a significant reduction on days 6 and 7. On days 6 and 7, the albumin production of HepG2 C3A Static Function Control was much less than the rocked device.

The synthesis of urea when cultured in the rocked device under bidirectional fluidic flow versus static cell cultures was measured. Significant differences were observed between the rocked device and the Multi-cell line Static Function Control on days 3–6 (Fig. 6B). Both groups showed an overall gradual increase but the Multi-cell

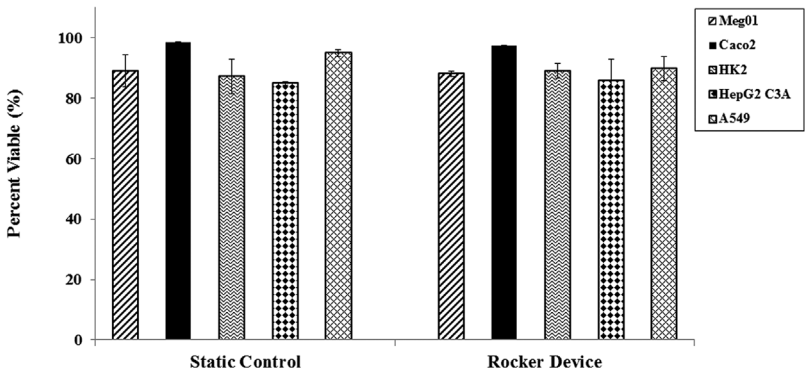


**Figure 4.** Viability in the 14 Chamber Rocked Device versus Static Viability Controls. Seven day viability of five cell lines (Meg01, Caco2, HK2, HepG2-C3A, and A549) maintained together in static chambers compared to being maintained in the 14 chamber rocked device ($n = 3$). Values are shown as the average percent viable ($n = 3$). Values are means + SEM.

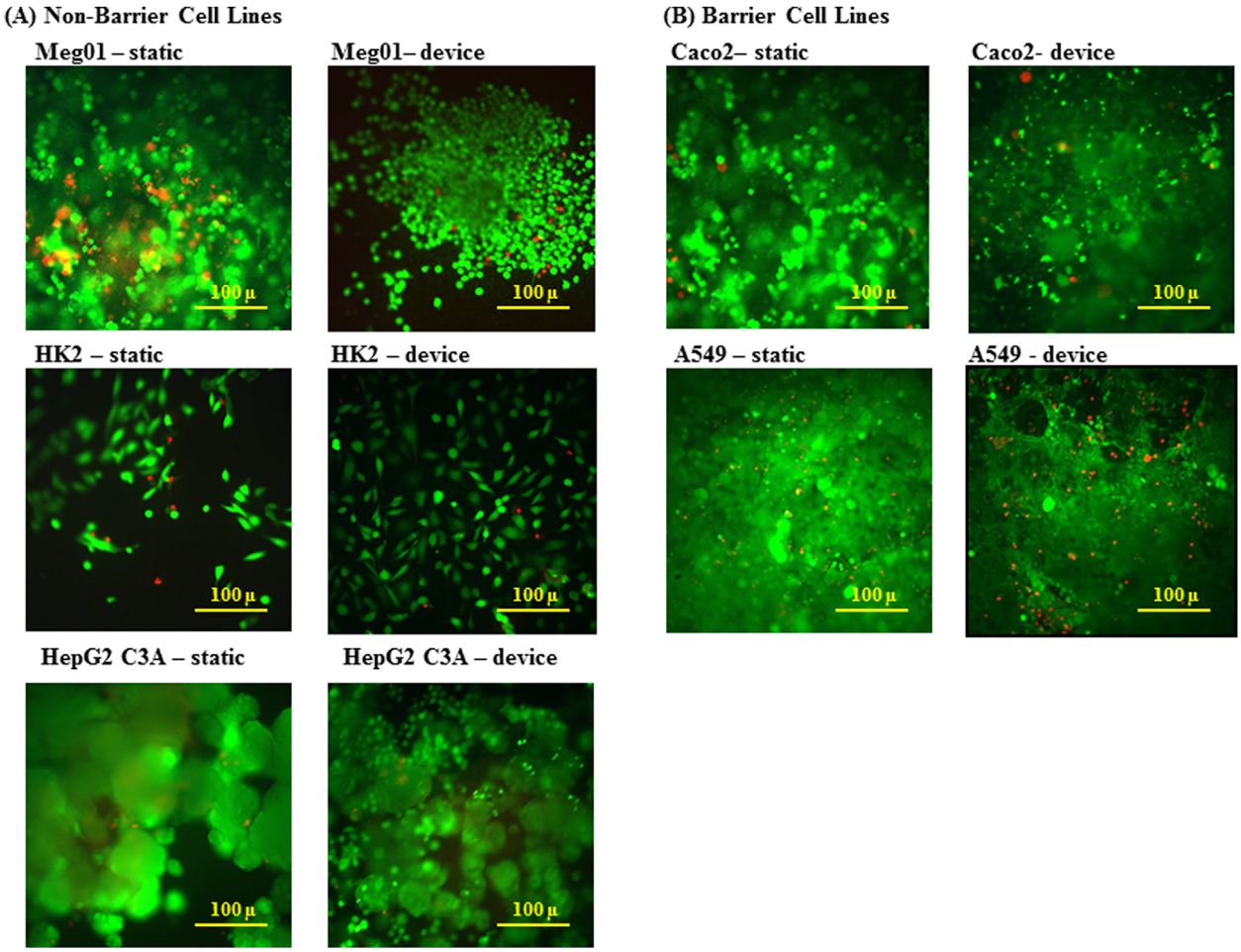


**Figure 5.** Fluorescent Micrographs (100× magnification) of 7 day viability of five cell lines (Caco2, A549, Meg01, HK2, and HepG2-C3A) maintained in static chambers or in the 14 chamber rocked device (using fluorescent Live/Dead Stain). Scale bars are present on the micrographs. (**A**) Non-Barrier cell lines (Meg01, HK2, and HepG2-C3A) comparison (**B**) Barrier cell lines (Caco2 and A549) comparison ($n = 3$).

line Static Function Control showed decreases on days 5 and 6. Significant differences were observed between the Multi-cell line Static Function Control and the Single-cell line Static Function Controls.

To evaluate whether our rocked device would be suitable for drug testing, we monitored CYP1A1 and CYP3A4 activity on 7 day. We measured induced CYP1A1 activity in the rocked device, the Multi-cell line Static Function Control, and all of the Single-cell line Static Function Control groups except for HK2. We were not able to measure noninduced CYP1A1 activity in the Caco2, A549, Meg01, and HK2 Single-cell line Static Function Control groups because it was below our assay's detection capability. The measured activity of CYP1A1 of the induced rocked device, the induced HepG2 C3A Static Function Control and the induced Multi-cell line Static Function Control were similar. However, the Multi-cell line Static Function Control had a significantly higher noninduced value than the other two groups creating significant differences in the induced/noninduced ratios of CYP1A1 activity (Fig. 6C).

We also measured induced CYP3A4 activity in the rocked device, the Multi-cell line Static Function Control, and three of the Single-cell line Static Function Control groups (Caco2, A549, and HepG2 C3A). We were not able to measure induced or noninduced CYP3A4 in the Meg01 or HK2 Single-cell line Static Controls because it was below our assay's detection capability. The actual CYP3A4 activity from the induced rocked device, the induced HepG2 C3A Static Function Control and the induced Multi-cell line Static Function Control were similar. However, the Multi-cell line Static Function Control had a higher noninduced value than the other groups creating a difference in the induced/noninduced ratios (Fig. 6C). Significant differences were observed between the induced Multi-cell line Static Function Control and the induced Caco2 Static Function Control as well as between the Multi-cell line Static Function Control and the induced A549 Static Function Control.

To further characterize the rocked device and compare to our controls, we opened the devices on day 7 and the barrier cell lines from the rocked device, the Multi-cell line Static Function Control, A549 Static Function Control and Caco2 Static Function Control were immunostained for tight junctions and surfactant (Fig. 7). The amount of surfactant appeared to be somewhat greater in the static systems than the rocker device and the nuclei appeared smaller in

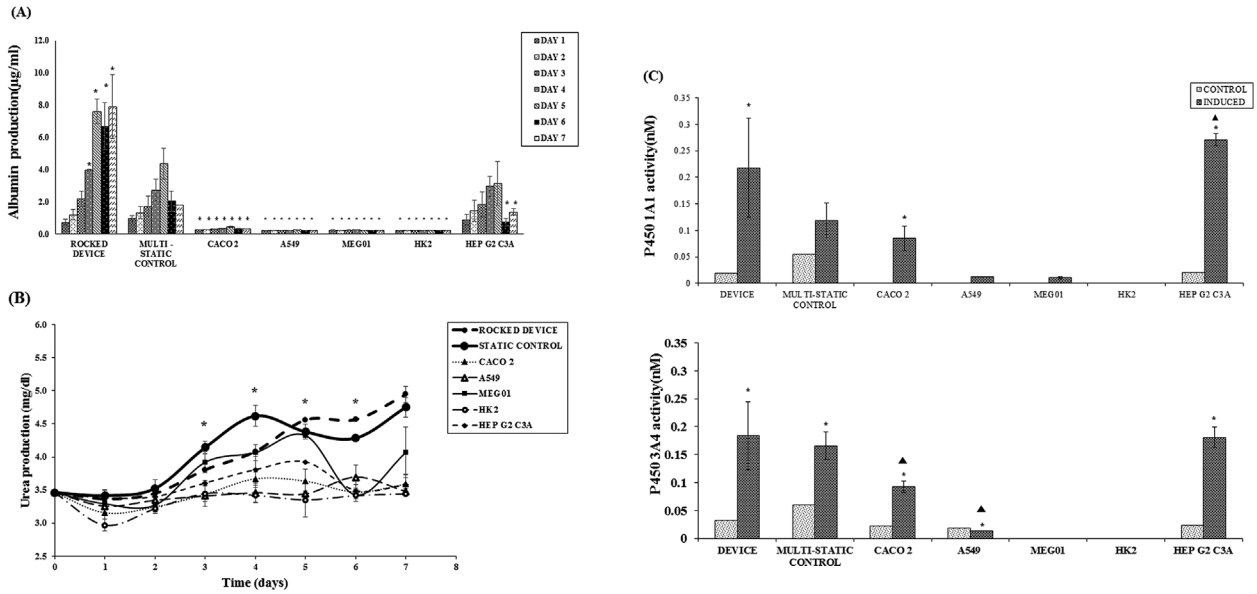


**Figure 6.** Functionality of the Rocked Device versus Multi-cell line Static Function Control and Single-cell line Static Function Controls. (**A**) Albumin production of the rocked device, the Multi-cell line Static Function Control and the Single-cell line Static Controls over a 7 day period. Each sample was run in duplicate. Values are means + SEM. Significant differences ($P < 0.05$) between Multi-cell line Static Function Control versus rocked device or Single-cell line Static Function Controls are indicated with an asterisk (*). (**B**) Urea production of the rocked device, the Multi-cell line Static Function Control and the Single-cell line Static Function Controls over a 7 day period. Each sample was run in duplicate. Values are means + SEM. Only the significant differences ($P < 0.05$) between Multi-cell line Static Function Control versus the rocked device are indicated with an asterisk (*). (**C**) CYP1A1 and CYP3A4 enzyme activity (nM) on day 7. Induced CYP activities are compared the uninduced CYP groups. Each sample was run in duplicate. Values are means + SEM. Please note that the replicates of the uninduced levels were close together so the SEM are not observed on the graph. The significant differences ($P < 0.05$) using a two tailed Student *t*-test between the individual induced versus uninduced groups are indicated with an asterisk (*). The significant differences ($P < 0.05$) using a two tailed Student *t*-test between the induced Multi-cell line Static Function Control and the other groups are indicated with a triangle (▲).

the static systems. The level of ZO-1 in the static systems also appeared to be more continuous that in the rocked system.

## Discussion

We characterized a bidirectional flow, pumpless, multi-chamber device that can be used to study interactions between different cell/tissue types whose numbers are physiologically proportional. This two chamber layer device was designed so that top layer contained open barrier chambers and reservoirs providing direct access to the circulation or entry after passing through the lung chamber, GI chamber or the skin chambers. The second chamber layer contained the nonbarrier tissues that were embedded in a hydrogel (PGMatrix) providing a 3D model of the body's solid organs.

The gaskets with the channels were designed to cross the cell containing chambers and connect the two medium reservoirs. The channel depths were constant at 0.25 mm because it was the thickness of the PMMA and the course of the channels was modeled as a straight rectangular duct. The simple design of the channels was desired to avoid dead or stagnant areas in the channels (corner effects). The channel widths were calculated from the desired volumetric flow rates and the cross-sectional area required to obtain that flow rate (Table I). These desired volumetric and linear flow rates were determined for each channel/chamber individually based on the human physiological data presented in the literature (Table I) (Haber et al., 2013; Price et al., 2003).

We performed a variety of fluid distribution tests in the device. First, the overall device mixing was observed to be complete if we set the rocker to 60 s with one side up then 60 s with the other side up program as we were able to obtain equilibration of a tracer across the two reservoirs within 20 min (Fig. 3B) but not with the 30 s program. Secondly, we observed that the chambers with hydrogel and reservoirs could be cleared of a diffusible dye (trypan blue) in 10 min or less. This observation suggests that exposure of the device to a diffusible reagent that does not bind irreversibly to surfaces can be cleared from the system within a reasonable time.

The observed volumetric and observed linear flow rates for 11 channels were compared to our calculated flow rates. It was expected that with a large number of channels and passive flow that the control of flow balancing between channels would be sensitive to small changes and imperfections in the device. The observed flow rates (Table II) were compared to the calculated target values. The channels flow rates were 15% within the calculated, except for heart, spleen, pancreas, and bone marrow. The discrepancy in some of the flow rates could be due to factors such as channel imperfections and the laser cutting accuracy of the channels ($\pm 100$ μm). The flow rate calculations depend upon the radius of the channel being raised to the fourth power so small changes in the radius could lead to large differences in the flow rates, especially in the small channels. However, the flow pattern was easily replicated among the multiple devices that we had. Possible ways to improve the accuracy of flow rates through the channels would be to decrease the angle of the

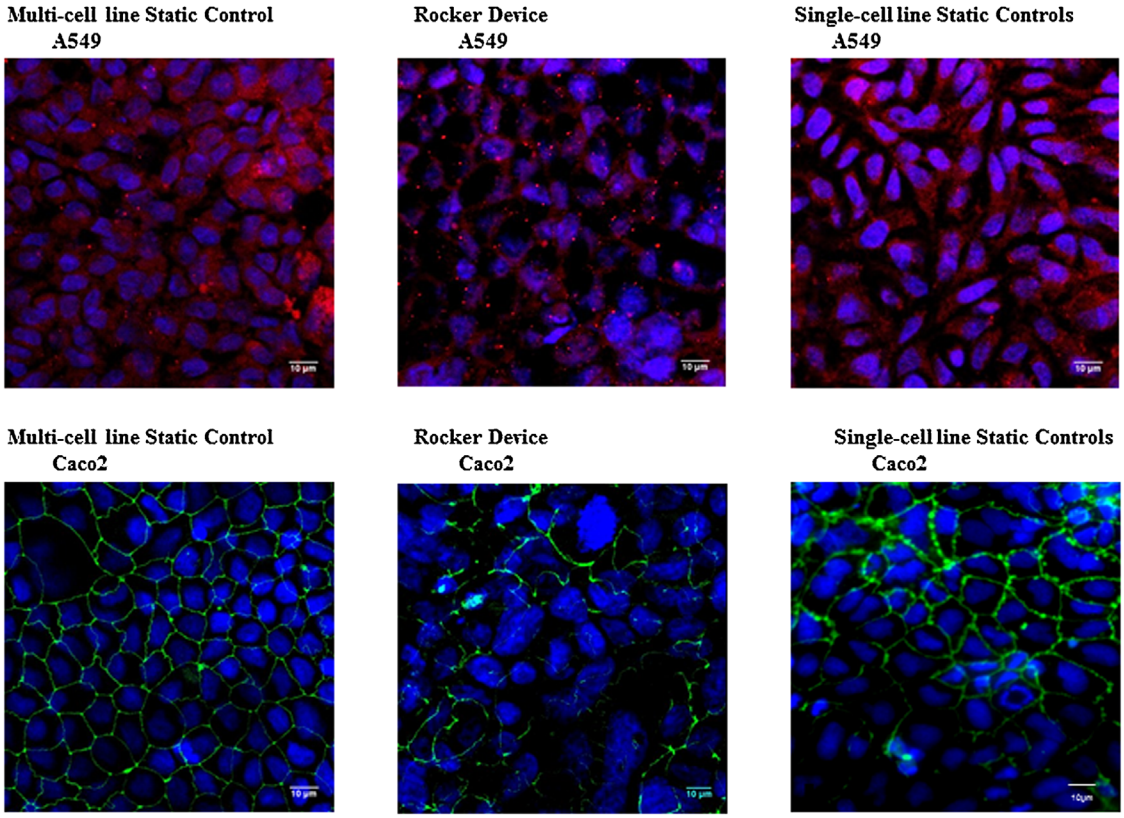


**Figure 7.** Immunostaining of Cells in the Rocked Device, Multi-cell line Static Function Control, and Single-cell line Static Function Controls. Fluorescent confocal images of the nonbarrier cell lines (A549 and Caco2) were observed after immunostaining for surfactant (red) and tight junctions (protein ZO-1, green). The nuclei were counter-stained (DAPI, blue). The cultures were observed under a water immersion 25× collared objective and further magnified with the Zen program. Scale bars are present on the micrographs.

rocker platform used (adjusting channel sizes accordingly) to minimize diffusion effects or use a fabrication technique of the channel gaskets that would provide a more accurate width and height of the channel.

Our preliminary studies using HepG2 C3A cells in all 14 compartments demonstrated that over 2 days all compartments sustained high cell viability (>85%) in all chambers. This observation is critical because it demonstrates that the device could sustain cells in all of the chambers simultaneously. We believe that HepG2 C3A is a good representative cell line because of its high demand for nutrients and is a metabolically active cell line. Other cells that are less metabolically active than HepG2 C3A should work as well. This experiment demonstrates that all 14 compartments are capable of sustaining cells and there is a good possibility that it would be possible to populate all compartments with cells to represent the corresponding organs.

After choosing five cell lines to represent both of our desired tissue types (barrier and nonbarrier), we demonstrated that these cell lines (Caco2, A549, HepG2 C3A, HK2, and Meg01) could be maintained separately and together in a common medium for more than 7 days. The cell cultures were grown as monolayers (2D) and/or resuspended in a hydrogel (PGMatrix) (3D). The viability in the monolayer and gel entrapped cultures for the nonbarrier cells were comparable to each other. There was some variability observed between the two viability measurement methods. This may be explained by the fact that the fluorescent live/dead kit used area to determine the % viable as opposed to using the exact cell number when using trypan blue exclusion and a hemocytometer. However, the overall viability across all five cell lines using either method was still 80% or better when growing cells as a monolayer or embedded in hydrogel static cultures.

Five cell culture lines were used to demonstrate that we could obtain comparable viability in our rocked device for 7 days versus a 7 day Static Viability Control. We plated two cell lines (Caco2 and A549) in the appropriate barrier chambers to represent the GI and lung tissues and three cell lines (Meg01, HK2, and HepG2 C3A) in PGMatrix in the appropriate nonbarrier chambers to represent the bone marrow, kidney, and liver. Cell viability, determined by using Invitrogen's Live/Dead Stain, was above 85% for both the rocker device and Static Viability Control and there was no significant difference observed when comparing the individual chambers (Fig. 4). The maintenance of high viability in the device with much less medium (4.7 mL) than the static system (60 mL) validates the plausibility of the device design and operation. This finding demonstrated that the device was not detrimental to the cells. The benefits of using the cells in the device versus a static system is that the rocked device simulates the flow rates of blood in the body and may provide more

accurate means of predicting responses of the body to chemicals by mimicking the time dependent exchange of metabolites between compartments.

We did not attempt longer studies because the cell culture lines tend to continue to proliferate in this medium and possibly at different rates. If these cell lines were to be considered for longer studies a medium with decreased serum concentration or the use a serum-free medium to slow proliferation should be considered. The use of primary cells in a medium that sustains viability but does not promote growth could also be used for longer studies, because of their reduced proliferation rate.

We demonstrated (Fig. 6) that the cells in the rocked device retain cellular function throughout the 7 days. In fact, when compared to either the Multi-cell line Static Function Control or the Single-cell line Static Function Controls, high cellular activity as determined from albumin production was sustained better in the rocked device on days 6 and 7. Urea production was similar between the Multi-cell line Static Function Control and rocked device. In the rocked device significant induction of CYP1A1 and CYP3A4 activities was observed indicating maintenance of functionality which is also crucial activity for drug and chemical metabolism. The level of activity was similar to that of the HepG2 C3A Static Function Control and not statistically different from the Multi-cell line Static Function Control.

Immunostaining was another analytical method that was used in the rocked device. One can disassemble the device and stain with antibodies or perform live/dead assays with success. The barrier cell lines of our experimental groups were stained for surfactant or tight junctions. Fluorescent labeling was a useful means to observe cells because cells grown on porous membranes are normally difficult to see. The amount of surfactant from the A549 cells appeared to be somewhat greater in the static systems than the rocked device. A possible explanation is that the fluid flow in the rocked device maybe causing a more uniform spreading of the surfactant and might be able to provide better means of reducing the surface tension of the cells than the static system. The level of ZO-1 in the static systems also appeared to be more continuous than in the rocked system. Again the fluid flow might be moving the porous membrane causing some disruption in the cellular connections.

Most importantly we showed that it is possible to construct a microphysiological system with a large number of cell containing chambers where cells remain not only viable, but also display functionality. These models can be constructed to sustain physiologically relevant relationships among pseudo-organ like chambers. Since many labs are currently constructing tissue engineered constructs that mimic organ functions it should be possible to populate all of the 13 organ compartments in this type of device with living artificial tissues. Many of these tissues will be based on induced pluripotent stem cells or primary cells, rather than cell lines. What we have demonstrated here is a physical framework in which these tissue or organ mimics can be integrated to capture some of the interactions among organs in the human body when challenged with drugs or chemicals. Since the physical model emulated a PBPK, the results of such experiments could be incorporated into a corresponding mathematical model to guide additional experiments (Shuler, 2012).

Financial support for this work was provided in part by an anonymous gift to Cornell and in part through the National Center for Advancing Translational Sciences at the National Institutes of Health (UH2TR000156-01). Laser cutting of the 14 chamber rocker device' s channel and chamber gaskets was performed under the guidance of Beth Rhoades at the Cornell NanoScale Science and Technology Facility, a member of the National Nanotechnology Infrastructure Network, which is supported by the National Science Foundation (Grant ECS-0335765). Confocal microscopy was performed on the Zeiss LSM 710 Confocal under the guidance of Johanna Cruz at the Imaging Facility, Cornell's Biotechnology Resource Center that is supported by the NIH (1S10RR025502). The frame of this device was milled out of a polycarbonate sheet by Glenn Swan on a CNC Bridgeport Milling Machine at Cornell University. Shuler is CEO of Hesperos, Inc. which builds and uses microphysiological systems for use by pharmaceutical firms to test potential drug candidates in human microphysiological systems, although this study is independent of Hesperos, Inc.

## References

Abbott A. 2003. Cell culture: Biology's new dimension. Nature 424:870–872.

Bhatia S, Ignber DE. 2014. Microfluidic organs-on-chips. Nat Biotechnol 32:760–772.

Brown RP, Delp MD, Lindstedt SL, Rhomberg LR, Beliles RP. 1997. Physiological parameter values for physiologically based pharmacokinetic models. Toxicol Ind Health 13(4):407–484.

Cook D, Brown D, Alexander R, March R, Morgan P, Satterthwaite G, Pangalos MN. 2014. Lessons learned from the fate of AstraZeneca's drug pipeline: A five-dimensional framework. Nat Rev Drug Discov 13:419–431.

Davies B, Morris T. 1993. Physiological parameters in laboratory animals and humans. Pharm Res 10(7):1093–1095.

El-Ali J, Sorger PK, Jensen KF. 2006. Cells on chips. Nature 442:403–411.

Esch MB, Smith A, Prot JM, Oleaga C, Hickman J, Shuler ML. 2014a. How multi-organ microdevices can help foster drug development. Adv Drug Deliv Rev 69–70:158–169.

Esch MB, Mahler GJ, Stokol T, Shuler ML. 2014b. Body-on-a-chip simulation with gastrointestinal tract and liver tissues suggests that ingested nanoparticles have the potential to cause liver injury. Lab Chip 14(16):3081–3092.

Esch MB, Prot J-M, Wang YI, Miller P, Applegate D, Shuler ML. 2015. Pumpless microfluidic organ-on-a-chip: 3D human primary liver cell culture elevates metabolic activity under gravity-driven medium flow that periodically changes direction. Lab Chip 15:2269–2277.

Gerlowski LE, Jain RK. 1983. Physiological based pharmacokinetic modeling: Principles and applications. J Pharm Sci 72:1103–1127.

Ghanem A, Shuler ML. 2000. Combining cell culture analogue reactor designs and PBPK models to probe mechanisms of naphthalene toxicity. Biotechnol Prog 16:334–345.

Greek R, Menache A. 2013. Systematic reviews of animal models: Methodology versus epistemology. Int J Med Sci 10:206–221.

Haber S, Clark A, Tawhai M. 2013. Blood flow in capillaries of the human lung. J Biomech Eng 135(10):101006–101017.

Huh D, Torisawa Y, Hamilton GA, Kim HJ, Ingber DE. 2012. Microengineered physiological biomimicry: Organs-on-chips. Lab Chip 12:2156–2164.

Imura Y, Sato K, Yoshimura E. 2010. Micro total bioassay system for ingested substances: Assessment of intestinal absorption, hepatic metabolism, and bioactivity. Anal Chem 82(24):9983–9988.

Kirby BJ. 2013. Micro- and nanoscale fluid mechanics: Transport in microfluidic devices. New York: Cambridge University Press. p 46–75.

Lancaster MA, Renner M, Martin CA, Wenzel D, Bicknell LS, Hurles ME, Homfray T, Penninger JM, Jackson AP, Knoblich JA. 2013. Cerebral organoids model human brain development and microcephaly. Nature 501(7467):373–379.

Lin JH, Lu AYH. 1997. Role of pharmacokinetics and metabolism in drug discovery and development. Pharmacol Rev 49:403–449.

Mahler GJ, Esch MB, Glahn RP, Shuler ML. 2009. Characterization of a gastrointestinal tract microscale cell culture analog used to predict drug toxicity. Biotechnol Bioeng 104:193–205.

Maschmeyer I, Lorenz AK, Schimek K, Hasenberg T, Ramme AP, Hubner J, Lindner M, Drewell C, Bauer S, Thomas A, Sambo NS, Sonntag F, Lauster R, Marx U. 2015. A four-organ-chip for interconnected long-term co-culture of human intestine, liver, skin and kidney equivalents. Lab Chip 15:2688–2699.

Morier P, Vollet C, Michel PE, Reymond F, Rossier JS. 2004. Gravity-induced convective flow in microfluidic systems: Electrochemical characterization and application to enzyme-linked immunosorbent assay tests. Electrophoresis 25:3761–3768.

Nakao Y, Kimura H, Sakai Y, Fujii T. 2011. Bile canaliculi formation by aligning rat primary hepatocytes in a microfluidic device. Biomicrofluidics 5(2): 22212.

Nalayanda DD, Puleo C, Fulton WB, Sharpe LM, Wan T-H, Abdullah F. 2009. An open-access microfluidic model for lung-specific functional studies at an air-liquid interface. Biomed Microdevices 11(5):1081–1089.

Natarajan A, Stancescu M, Dhir V, Armstrong C, Sommerhage F, Hickman JJ, Molnar /familyName> P. 2011. Patterned cardiomyocytes on microelectrode arrays as a functional, high information content drug screening platform. Biomaterials 32:4267–4274.

Perry RH, Chilton CH. 1973. Chemical engineers' handbook. New York: McGraw-Hill Section 5. p 1–52.

Price PS, Conolly RB, Chaisson DF, Gross EA, Young JS, Mathis ET, Tedder DR. 2003. Modeling interindividual variation in physiological factors used in PBPK models of humans. Crit Rev Toxicol 33:469–503.

Sato T, Clevers H. 2013. Growing self-organizing mini-guts from a single intestinal stem cell: Mechanisms and applications. Science 340:1190–1194.

Shuler ML. 2012. Modeling life. Ann Biomed Eng 40(7):1399–1407.

Sin A, Chin KC, Jamil MF, Kostov Y, Rao G, Shuler ML. 2004. The design and fabrication of three-chamber microscale cell culture analog devices with integrated dissolved oxygen sensors. Biotechnol Prog 20:338–345.

Smith A, Long CJ, Berry BJ, McAleer C, Stancescu M, Molnar P, Miller PG, Esch MB, Prot J-M, Hickman JJ, Shuler ML. 2013. Microphysiological systems and low-cost microfluidic platform with analytics. Stem Cell Res Ther 4(suppl 1):S9.

Sung JH, Srinivasan B, Esch MB, McLamb WT, Bernabini C, Shuler ML, Hickman J. 2014. Using physiologically-based pharmacokinetic-guided "body-on-a-chip" systems to predict mammalian response to drug and chemical exposure. Exp Biol Med 239:1225–1239.

Sung JH, Esch MB, Prot J-M, Long CJ, Smith A, Hickman JJ, Shuler ML. 2013. Microfabricated mammalian organ systems and their integration into models of whole animals and humans. Lab Chip 13:1201–1212.

Sung JH, Kam C, Shuler ML. 2010. A microfluidic device for pharmacokinetic-pharmacodynamic (PK-PD) model on a chip. Lab Chip 10:446–455.

Sung JH, Shuler ML. 2009. A micro cell culture analog with 3-D hydrogel culture of multiple cell lines to assess metabolism-dependent cytotoxicity of anti-cancer drugs. Lab Chip 9:1385–1394.

Sweeney LM, Shuler ML, Babish JG, Ghanem A. 1995. A cell culture analogue of rodent physiology: Application to naphthalene toxicology. Toxicol In Vitro 9(3):307–316

Tatosian DA, Shuler ML. 2009. A novel system for evaluation of drug mixtures for potential efficacy in treating multidrug resistant cancers. Biotechnol Bioeng 103:187–198.

Viravaidya K, Sin A, Shuler ML. 2004. Development of a microscale cell culture analog to probe naphthalene toxicity. Biotechnol Prog 20:316–323.

Wagner I, Materne E-M, Brincker S, Suβbier U, Fradrich C, Busek M, Sonntag F, Sakharoz DA, Trushkin EV, Tonevitsky AG, Lauster R, Marx U. 2013. A dynamic multi-organ-chip for long-term cultivation and substance testing proven by 3D human liver and skin tissue co-culture. Lab Chip 13:3538–3547.

Whitesides GM. 2006. The origins and the future of microfluidics. Nature 442:368–373.

Zhang C, Zhao Z, Abdul Rahim NA, van Noort D, Yu H. 2009. Towards a human-on-chip: Culturing multiple cell types on a chip with compartmentalized microenvironments. Lab Chip 9:3185–3192.

## Supporting Information

Additional supporting information may be found in the online version of this article at the publisher's web-site.